Non-stationary Gaussian models with physical barriers

Haakon Bakka [a],[*], Jarno Vanhatalo [b], Janine B. Illian [c], Daniel Simpson [d], Håvard Rue [e]

[a] Statistics Program, CEMSE Division, King Abdullah University of Science and Technology, Thuwal 23955, Saudi Arabia
[b] Department of Mathematics and Statistics, Faculty of Science, and Organismal and Evolutionary Biology Research Programme, Faculty of Bio- and Environmental Sciences, University of Helsinki, Gustaf Häströmin katu 2b, P.O. Box 68, FIN-00014 University of Helsinki, Finland
[c] Centre for Research into Ecological and Environmental Modelling, School of Mathematics and Statistics, University of St Andrews, The Observatory, Buchanan Gardens, St Andrews, Fife, KY16 9LZ, Scotland, UK
[d] Department of Statistical Sciences, University of Toronto, 100 St. George Street, Toronto, Ontario, Canada, M5S 3G3
[e] Statistics Program, CEMSE Division, King Abdullah University of Science and Technology, Thuwal 23955, Saudi Arabia

ARTICLE INFO

ABSTRACT

The classical tools in spatial statistics are stationary models, like the Matérn field. However, in some applications there are boundaries, holes, or physical barriers in the study area, e.g. a coastline, and stationary models will inappropriately smooth over these features, requiring the use of a non-stationary model.

We propose a new model, the Barrier model, which is different from the established methods as it is not based on the shortest distance around the physical barrier, nor on boundary conditions. The Barrier model is based on viewing the Matérn correlation, not as a correlation function on the shortest distance between two points, but as a collection of paths through a Simultaneous Autoregressive (SAR) model. We then manipulate these local dependencies to cut off paths that are crossing the physical barriers. To make the new SAR well behaved, we formulate it as a stochastic partial differential equation (SPDE) that can be discretised to represent the Gaussian field, with a sparse precision matrix that is automatically positive definite.

* Corresponding author.
E-mail addresses: bakka@r-inla.org, haakon.bakka@kaust.edu.sa (H. Bakka), jarno.vanhatalo@helsinki.fi (J. Vanhatalo), jbi@st-andrews.ac.uk (J.B. Illian), simpson@utstat.toronto.edu (D. Simpson), haavard.rue@kaust.edu.sa (H. Rue).

The main advantage with the Barrier model is that the compu-
tational cost is the same as for the stationary model. The model is
easy to use, and can deal with both sparse data and very complex
barriers, as shown in an application in the Finnish Archipelago
Sea. Additionally, the Barrier model is better at reconstructing the
modified Horseshoe test function than the standard models used
in R-INLA.

1. Introduction

1.1. Background

Spatial Gaussian fields (SGFs) are widely used as model components when building spatial or
spatio-temporal models for a variety of applications, e.g. in the Generalised Additive model (GAM)
framework. These spatial model components are used to model the residual spatial structure, resulting
from unmeasured spatial covariates, spatial aggregation, and spatial noise. In applications where no
suitable covariates are available, the SGF and the intercept may be the only components in the model.

SGFs, also known as Gaussian fields or Gaussian random fields, are usually assumed to be stationary
and isotropic. An SGF is stationary if the model component does not change when the underlying
map is moved. Similarly, isotropy implies that the model component does not change when the
map is rotated. For convenience, we will use the word stationary to include both stationarity and
isotropy, and also for discrete approximations of these models. Using a stationary SGF implies the
assumption that any non-stationarity in the data are covered by the other model components, e.g. by
the spatial covariates, or that the data is stationary. However, when there are physical barriers, or
holes, in the study area, stationarity is an unrealistic assumption, as moving/rotating the map changes
the locations of these features, and should change the model. In this case, the dependency between
two observations should not be based on the shortest Euclidean distance between the locations, but
should take into account the effect of physical barriers, and "smooth around" them.

1.2. Motivating example

The motivating example we use in this paper is an archipelago on the south-west coast of Finland,
see Fig. 1, analysed by Kallasvuo et al. (2017) and re-analysed in Section 5. This example is both
complex enough to motivate a general solution and it contains many common features, including
peninsulas, inlets and islands of many different sizes. A stationary SGF would smooth over peninsulas
and islands, creating an unrealistic dependence structure for aquatic animals, and so, a non-stationary
model seems more appropriate.

We will refer to the problem of physical barriers that need to be taken into account by the SGF as the
coastline problem to simplify the language, not implying that we only consider coastlines to be valid
examples of the coastline problem. Other examples of physical barriers include roads, power lines,
mountains, and areas with different land use, and the models we discuss are able to deal with any
of these. Further, we will assume that *water* is the normal area, and *land* is the physical barrier; this
terminology needs to be reversed when we model data on land. Additional examples of the coastline
problem can be found in the introductions by Wood et al. (2008) and by Scott-Hayward et al. (2014).

1.3. Expanding the problem formulation

Another issue in the context of the coastline problem is what we refer to as the *boundary
polygon selection process*, explained through the following example. A researcher desiring to model
observations near the coast must represent the coastline with a polygon, as in Fig. 1. However,
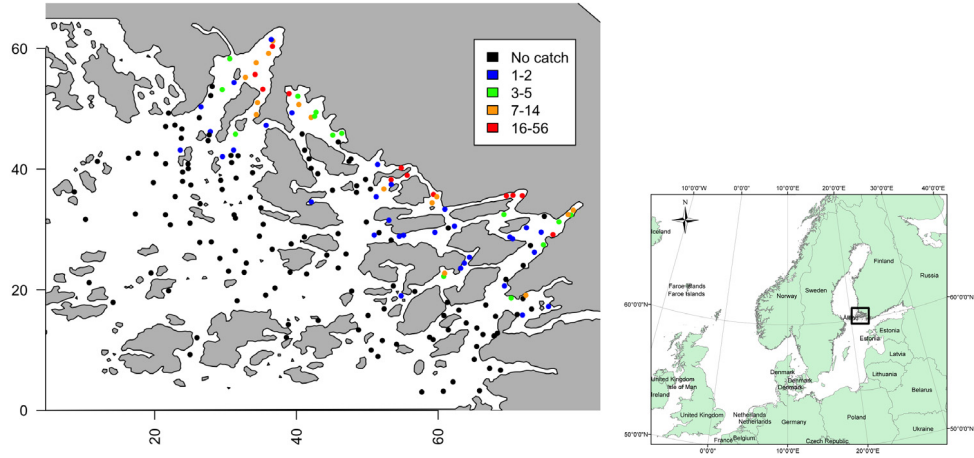
Fig. 1. The Archipelago Sea with an example dataset on counts of smelt larvae. The grey region is land and the white region is water. This study area has many islands and peninsulas, which we do not want the spatial model component to smooth over. The spatial axes are in kilometres.
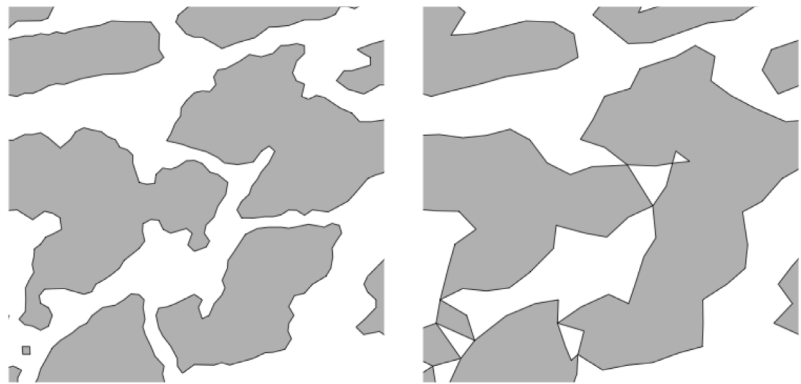
Fig. 2. Two approximations of the same coastline, at two different resolutions. Computing the shortest distances between locations in the left plot is very different from computing shortest distances in the right plot, as the East-West channel has disappeared completely. This example is a small cut-out of the study area in Fig. 1.

coastlines are often thought of as fractal-like, in the sense that any finite approximation will not be accurate, hence, different researchers are likely to use a different approximation for the same coastline polygons, see Fig. 2 for an example. Additionally, high and low tide may change the definition of the coastline. The spatial models constructed from two polygons should differ slightly, but not dramatically. If the same model, with a slightly different coastline approximation, results in different interpretations of results and predictions, the model looses its scientific credibility.

1.4. Literature review

There have been several approaches to the coastline problem that focus on computing the shortest distance in water; Wang and Ranalli (2007) develop the GLTPS from the Thin Plate Spline, Scott-Hayward et al. (2014) develop the CReSS as an improvement to the GLTPS, and Miller and Wood (2014) embed the data in a higher dimensional space where the new Euclidean distances are close to

the shortest distance in water, creating the MDSDS model. A strength of the GLTPS and CReSS is that they have a flexibility parameter determining the distance at which information is assumed to have a spatial dependency, which also determines the distance at which observations no longer noticeably influence predictions through the SGF. One weakness of these approaches is that they are significantly more cumbersome and time consuming to use than their stationary alternatives. Furthermore, the concept "shortest distance in water" is not a robust concept; this distance would change abruptly between the plots in Fig. 2. In this paper we do not consider any of these to be valid solutions to the stated problem, as they are not robust to the boundary polygon selection process.

Three other approaches are based on defining boundary conditions. Ramsay (2002) develop the FELSPLINE, which uses a smoothing penalty together with Neumann boundary condition (height-curves are orthogonal to the boundary). One strength of this approach lies in the use of Finite Element Method (FEM) which gives a good approximation of the smoothness penalty for irregular observations. The default SGF by Lindgren et al. (2011), assuming the mesh is only constructed in water, also uses Neumann boundary conditions and FEM. A weakness with these approaches, as discussed in Wood et al. (2008) and in Section 4 is that the Neumann boundary condition is often unrealistic and severely impacts on the results. Wood et al. (2008) develop the Soap-film smoother, and Sangalli et al. (2013) the SSR model, both models enabling the use of the Dirichlet boundary condition (a known value/function along the boundary). The main strength with the Dirichlet boundary condition is that when the true boundary values are known, not only will this give the correct result at the boundary, but the spatial field will smooth these values far into the water. As this condition acts like "perfect observations", observations near the boundary are not necessary for estimating the SGF near the boundary, and the result will have very narrow estimation intervals near the boundary. This strength is also a weakness: If the employed boundary condition is slightly wrong, the true intensity near the boundary is not covered by any estimation intervals, and in practice it is unlikely that the true boundary values are known explicitly. Indeed, in our guiding example (Fig. 1), we cannot use a Dirichlet condition of "no fish at the boundary" as this would imply that there are almost no fish close to the boundary either, which is clearly wrong. In the rare case when there is sufficient certainty about true value of the SGF at the boundary, as well as the propagation through the correlation structure of the SGF, we recommend using the Dirichlet condition, but for the rest of this paper we assume that the boundary values are unknown.

One way to remedy the weakness of the Dirichlet boundary condition is to put a separate model on the boundary, and then model the SGF conditionally on this boundary model, as Wood et al. (2008) do for the Soapfilm smoother. A strength of this approach compared to the simple Dirichlet approach is that it can reflect large uncertainties near the boundary. The model for the boundary, however, is very influential on the results near the boundary, and it is not clear what would constitute a good model for that role, nor how the model should change when the boundary is deformed. The main weakness of this approach is that it can fail to produce reliable models in cases with sparse data and complex boundaries. In our motivating example there are more islands than observation locations, which leads to a massive overparametrisation when creating a boundary model for each island.

1.5. Requirements for a new solution

Here, we set out five desirable properties of a solution to the coastline problem. These properties are inspired by the literature review and formulated to ensure that the main strengths of previous approaches are maintained, while the main weaknesses are overcome. We readily acknowledge that different scientists have different requirements for their models; we do not wish to imply that this list is the only possible list of requirements, but we recommend any reader who agree with this list to use the model we present in this paper. The SGF should

Property 1 be robust to the boundary polygon selection process,

Property 2 have a computational cost close to the stationary alternative,

Property 3 not be much more difficult for a researcher to use in practice, compared to the stationary GRF,
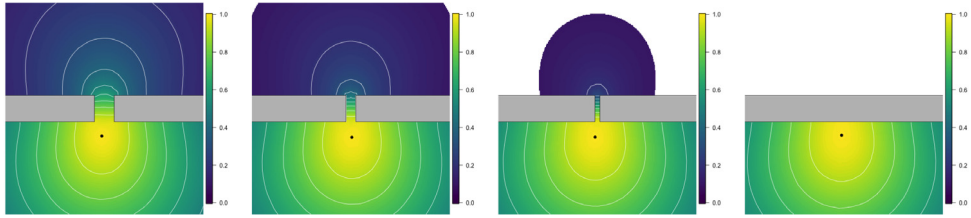
Fig. 3. Correlation plots of the SGF in Lindgren et al. (2011) where there is an opening in the land barrier. All parameters in the three plots are the same, except the gap widths, which takes the values 0.4, 0.2, 0.1, and 0.

Property 4 include a flexibility parameter, a *range* parameter, determining the distance of spatial similarity, as described below, and,

Property 5 not introduce any new assumptions that are not realistic.

Property 1 was discussed in Section 1.3. In Fig. 3 we illustrate the behaviour of the default SGF with Neumann boundaries in Lindgren et al. (2011) when modelling a small channel in a coastline. As the channel becomes smaller, and is eventually closed, the dependency between the south and the north shrinks towards zero. This illustrates that the behaviour of this model component depends continuously on the width of the channel, hence we believe it is robust to the boundary polygon selection process.

For Property 2, the computational cost is a clear bottleneck in many applications, as researchers need to fit several models to compare predictive performance and investigate the stability of inference results. We consider the $\mathcal{O}(n^3)$ cost of computing all possible distances between n datapoints, as used in e.g. Scott-Hayward et al. (2014), or even the $\mathcal{O}(n^2)$ cost of writing down the full spatial covariance matrix, to be too expensive for a general solution to the coastline problem.

Another important problem, although less well defined, is the cost of time for a researcher to employ the model in practice. Property 3 is of little interest from a mathematical point of view, but to achieve widespread use this property is essential. To reduce the effort needed, constructing the model component should be automatic, in the sense that there should be few, if any, additional specifications or computations that the user needs to do, and that the results should be numerically stable even for complex coastlines, such as in our motivating example. The SGF is often used as a nuisance parameter, so we should not add any new steps in model construction, compared to the stationary SGF, that need to be tuned and/or assessed by model comparison. Models constructed from this SGF should be able to fit both sparse and rich data, without having to consider whether the dataset is informative enough to do inference with a non-stationary SGF.

Property 4 was discussed in Section 1.4. This parameter increases flexibility in the sense that, if a user does not want to infer it from the data, it can instead be fixed to a constant; intrinsic smoothers can be recovered by letting this constant go to infinity.

Property 5 is a catch-all for avoiding new models with problematic behaviour. If, for example, we can solve the coastline problem by introducing an artificial partition of our dataset, or by moving the locations to arbitrary new locations, such an approach may satisfy Property 1 to 4, but should not be considered a valid approach. When new models are developed, as in this paper, we need to shed light on the behaviour of the model to the best of our ability. Common sense, or application experts, can then determine whether the assumptions introduced by the new approach are reasonable. Property 5 is the only property that the default model by Lindgren et al. (2011) does not satisfy; in Section 4 we show that the Neumann boundary condition is unrealistic and has a strong impact.

1.6. Outline of the paper

The rest of the paper is organised as follows. In Section 2 we motivate and define the Barrier model, a new approach to the coastline problem satisfying all of the stated properties. In Section 3 we

show how to construct the model component as a Gaussian precision matrix conditional on hyper-parameters. In Section 4 we run the standard modified horseshoe reconstruction problem (Wood et al., 2008), to compare the new model to the Neumann model and the stationary alternative. In Section 5 we analyse the motivating example, fish data from the Finnish Archipelago Sea. In the supplementary material we provide more details on all the models, and tutorials for how to use the Barrier model.

2. The barrier SGF

2.1. Background

One of the most widely used models for the SGF is the Matérn model (Whittle, 1954), with justification (e.g. Diggle, 2010), and applications varying from simple geostatistical models with Gaussian likelihoods to marked point patterns (Illian et al., 2012). The interest in applying the Matérn model seems to be increasing, partly because of the INLA approach (Rue et al., 2009) and the SPDE approach (Lindgren et al., 2011), as this enables fast Bayesian inference, and is relatively user friendly (see e.g. Blangiardo and Cameletti (2015) and Krainski et al. (2018)). A few notable examples include; analysing transmission intensity of malaria (Noor et al., 2014), modelling under-five and neonatal mortality (Golding et al., 2017), and assessing the impact of control measures on malaria in Africa (Bhatt et al., 2015).

The Matérn field is a Gaussian random field, i.e. a continuously indexed random variable where the indices are a subset of $\mathbb{R}^n$, and any finite collection of indices gives variables that are jointly multivariate Gaussian. We base the Barrier SGF on the Matérn model, in dimension 2, and, in the absence of land, it reduces to this model. We fix the smoothness parameter, as this parameter is in some cases not identifiable, choosing $\nu = 1$ as this value is both convenient to work with and provides reasonably smooth fields. We refer to Bolin and Kirchner (2018) and Bolin et al. (2017) for how to extend SPDE models to other values of ν.

One way to represent the Matérn field $u(s)$ is by giving the covariance as a function of distance between two points. Letting d be the distance between two arbitrary points, $d = \|s_i - s_j\|$, the covariance function is

$$C(d) = \sigma_u^2 \frac{d\sqrt{8}}{r} K_1\left(\frac{d\sqrt{8}}{r}\right). \tag{1}$$

Here, σ_u and r are constants, and K_1 is the modified Bessel function of the second kind. The subscript on σ_u clarifies that this is the marginal standard deviation of the model component u. Note that we have re-parametrised the traditional Matérn covariance function with range $r = \rho/\sqrt{8}$ where ρ is the traditional length scale parameter (see Lindgren et al. (2011)). The range r is interpretable because the correlation between two points that are r units apart is near 0.1, and r is approximately the smallest distance from high value to low value regions of a random sample from the SGF. If we were to follow previous approaches, and defined a shortest distance, we might try to replace the d in the above equation with an approximate shortest distance around land. This, however, would not satisfy Property 1.

2.2. Motivating the new approach

To motivate our approach we interpret the Matérn field as a Simultaneous Autoregressive (SAR) model on a grid giving an approximate representation (for a fixed range). Let $U_{i,j}$ be the random variable in grid cell $[i, j]$, and let $z_{i,j}$ be iid zero mean Gaussians,

$$U_{i,j} - k\left(U_{i-1,j} + U_{i,j-1} + U_{i+1,j} + U_{i,j+1}\right) = z_{i,j},$$

see Eq. (5) and onwards in Lindgren et al. (2011).

When interpreting the Matérn model in this way, the relevant "distance" is not the shortest distance, but rather a collection of all possible paths from one location to another; and the dependency between two points relies on all the paths that exist between them. Intuitively, what we want to do

is to remove the collection of paths crossing land; this also implies that the new distance will not be the new shortest distance, but will be an indirect result of the new collection of available paths. For computational reasons, we will not completely remove any paths, but instead weaken the dependency along those paths to almost zero.

The SAR model is defined for the entire area, including land. However, the SAR model over land only exists as a computational trick, and no fitting or prediction will be done on land. To illustrate the SAR model at the boundary between water and land, consider an example with a regular grid where land is to the right of origo, filling the space vertically, so grid cell $U_{1,0}$ is on land, while $U_{0,0}$ is not. The equation for the SAR model at $U_{0,0}$ then becomes

$$(1 - k_2)U_{0,0} - k\left(U_{-1,0} + U_{0,-1} + (1 - k_3)U_{1,0} + U_{0,1}\right) = z_{0,0},$$

where k_3 reduces the dependency ($k_3 < 1$), and k_2 can be used to make the SAR well behaved. Selecting the appropriate values for k_2 and k_3, for all the "SAR equations" near the boundary, would be an almost impossible task, if it was not for a link between SAR/CAR models and Matérn models through the stochastic partial differential equation (SPDE) approach (Lindgren et al., 2011), as explained below.

2.3. The barrier SGF

The stationary Matérn field is the (weak, stationary) solution $u(s)$ to the stochastic partial differential equation

$$u(s) - \nabla \cdot \frac{r^2}{8}\nabla u(s) = r\sqrt{\frac{\pi}{2}}\sigma_u \mathcal{W}(s), \tag{2}$$

where $u(s), s \in \Omega \subseteq \mathbb{R}^2$ is the Gaussian field, r and σ_u the same constants as in Eq. (1), $\nabla = \left(\frac{\partial}{\partial x}, \frac{\partial}{\partial y}\right)$, and $\mathcal{W}(s)$ denotes white noise. For further details, see Lindgren et al. (2011); we have re-parametrised their equation (2) and fixed $\alpha = 2$. Details on the interpretation of this SPDE and how to solve it through the FEM can be found in Bakka (2018).

On land we introduce a different Matérn field, with the same σ but a range close to zero, to remove the correlation there. The Barrier SGF $u(s)$ is the solution to

$$u(s) - \nabla \cdot \frac{r^2}{8}\nabla u(s) = r\sqrt{\frac{\pi}{2}}\sigma_u \mathcal{W}(s), \text{ for } s \in \Omega_n$$

$$u(s) - \nabla \cdot \frac{r_b^2}{8}\nabla u(s) = r_b\sqrt{\frac{\pi}{2}}\sigma_u \mathcal{W}(s), \text{ for } s \in \Omega_b, \tag{3}$$

where Ω_n is the normal area, Ω_b is land, i.e. the physical barrier, and their disjoint union gives the whole study area Ω. To achieve Property 2, we do not include additional parameters that require tuning, inference, or model assessment, and hence the parameter r_b is taken to be a fixed fraction of the range r, e.g. $r_b = r/10$. We choose the solution $u(s)$ that is continuous and satisfies the so-called "natural matching conditions" (see Gander and Dubois (2015) Section 5),

$$\frac{r^2}{8}\frac{\partial u_n}{\partial n_b} = \frac{r_b^2}{8}\frac{\partial u_b}{\partial n_b},$$

where $\frac{\partial u_n}{\partial n_b}$ is the partial derivative orthogonal to the boundary (i.e. in direction n_b) just inside the normal area, and $\frac{\partial u_b}{\partial n_b}$ is the same derivative just inside the land area.

To prove existence and uniqueness, we view the SPDE through operators on Hilbert spaces. Let $\Omega \subset \mathbb{R}^2$ be a polygonal domain, and H be the subspace of $L^2(\Omega)$ where all functions satisfy Neumann boundary conditions on Ω. The operator

$$L = \kappa(s) + \nabla \cdot a(s)\nabla,$$

with $\kappa, a \in L^\infty$, $\kappa(s) > \kappa_0 > 0$ and $a(s) > a_0 > 0$, is defined on $\dot{H}^2 = \mathcal{D}(L)$ which is dense in H.

Theorem 1. *The equation*

$$Lu = \mathcal{W},$$

has a unique solution $u \in L_2(\Pi; H)$, Π-a.s.

For proof, see Appendix A.

3. Finite dimensional representation of $u(s)$

In this section we detail how to represent the continuous GF $u(s)$ with a finite dimensional approximation, and how to compute the sparse precision matrix Q for the coefficients of this approximation. We use a linear finite element approach that approximates the solution with a (continuous) piecewise linear function, similar to Lindgren et al. (2011). This is to avoid any extra interpolation approximations after the solution is computed, which would be the case with a grid based approach.

We rewrite Eq. (3) to

$$\left[1 - \nabla \frac{r(s)^2}{8} \nabla \right] u(s) = r(s) \sqrt{\frac{\pi}{2}} \mathcal{W}(s)$$

$$r(s) = r_q \text{ on } \Omega_q,$$

where the domain Ω is a disjoint union of Ω_q for $q = 1, 2, \ldots, k$, and with Neumann boundary condition on $\partial \Omega$. This is a minor generalisation; we use $k = 2$ in the Barrier SGF.

Irregular outer boundaries are known to cause numerical artefacts and unrealistic behaviour, to avoid this issue we extend the study area and make it convex. This moves the boundaries away from the data, avoiding an impact of the boundary condition on the fitted model (see Lindgren et al. (2011) appendix A.4). Having a regular outer boundary is a common assumption for many numerical techniques and approximations (Grisvard, 1985), and inference can later be restricted back to the study area.

After a mesh has been selected, as in Fig. 4, the linear finite elements $\psi_i(s)$ are defined to be piecewise linear on this mesh, taking the value 1 in node i, and the value 0 in all other nodes. The spatial field approximation $\tilde{u}$ is then $\tilde{u}(s) = \sum_{i=1}^{n} u_i \psi_i(s)$, where n is the number of basis functions (one for each mesh node), and $\tilde{u}_i$ are Gaussian random variables, with precision matrix Q.

When solving this SPDE with finite elements, the equation is re-interpreted in the following weak form,

$$\left\langle \psi_j(\cdot), \left[1 - \nabla \frac{r(\cdot)^2}{8} \nabla \right] \tilde{u}(\cdot) \right\rangle = \left\langle \psi_j(\cdot), r(\cdot) \sqrt{\frac{\pi}{2}} \mathcal{W}(\cdot) \right\rangle, \tag{4}$$

meaning that the joint distribution, over j, of the left hand side is equal in distribution to the joint distribution on the right hand side. The inner product $\langle f, g \rangle = \int f(s)g(s) \, ds$.

Define the matrices

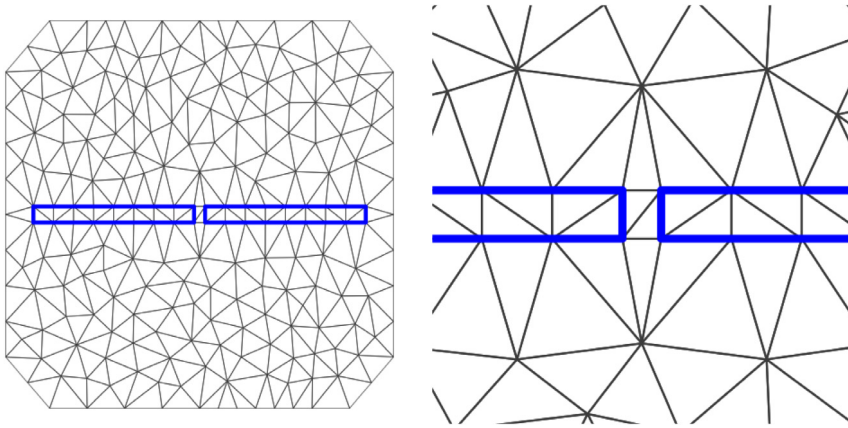$$J_{i,j} = \langle \psi_i, \psi_j \rangle = \int \psi_i(s)\psi_j(s) \, ds \tag{5}$$

$$(D_q)_{i,j} = \langle 1_{\Omega_q} \nabla \psi_i, \nabla \psi_j \rangle = \int_{\Omega_q} \nabla \psi_i(s) \nabla \psi_j(s) \, ds \tag{6}$$

$$(\tilde{C}_q)_{i,i} = \langle 1_{\Omega_q} \psi_i, 1 \rangle = \int_{\Omega_q} \psi_i(s) \, ds \tag{7}$$

which are the basic ingredients in the finite element method. Writing $\tilde{u}(s)$ as a linear combination of elements in Eq. (4), and putting the resulting coefficients into matrix form, we get $A\tilde{u} = \epsilon$ where

$$A = J - \frac{1}{8} \sum_{q=1}^{k} r_q^2 D_q \tag{8}$$

Fig. 4. Example mesh for a coarse version of the example in Figs. 3 and 6. The mesh has been extended to move the outer boundary far away from the region of interest, and the blue rectangles denote the land area. The second plot is a zoom-in of the first.

and ϵ is multivariate Gaussian with

$$\mathrm{Cov}(\epsilon) \approx \tilde{C} = \frac{\pi}{2} \sum_{q=1}^{k} r_q^2 \tilde{C}_q, \tag{9}$$

which is diagonal, making the ϵ_i independent. To get the approximation $\tilde{C}$ we follow the arguments of Lindgren et al. (2011). Since A is symmetric, $Q = A\tilde{C}^{-1}A$. For computational efficiency it is important to store the matrices J, C_q, and D_q so that Q can be computed quickly for new values of $(r_q)_q$.

The difference between a stationary SGF and the Barrier SGF can be understood from the D_q's, see Fig. 5 for an illustration. In this example,

$$D_1 = \begin{bmatrix} 3.0 & . & -0.5 & -0.5 \\ . & 3.0 & -0.5 & -0.5 \\ -0.5 & -0.5 & 3.0 & . \\ -0.5 & -0.5 & . & 3.0 \end{bmatrix}, \quad D_2 = \begin{bmatrix} 1.0 & 0.0 & -0.5 & -0.5 \\ 0.0 & 1.0 & -0.5 & -0.5 \\ -0.5 & -0.5 & 1.0 & . \\ -0.5 & -0.5 & . & 1.0 \end{bmatrix},$$

with $q = 1$ representing the white normal area, and $q = 2$ representing the green land area in the figure. The numbers in circles show the central location of each finite element, which corresponds to rows and columns in the matrices. The connection between element 1 and 2 is structurally zero in D_1 signified by a ".", since no white triangles are connecting node 1 and 2, while it is numerically zero in D_2 as the inner product of the derivatives is zero (Eq. (6)). Elements 3 and 4 share no triangles and so has structural zeros in both matrices. For nodes 3 and 4, 1/4 of the area of neighbouring triangles are green and the other 3/4 are white, and the triangles are symmetric around the node explaining the entries on the diagonals. The diagonal entries for node 1 and 2 are slightly more complicated, but can be found by computing the integrals.

In Fig. 6 we show that the new SGF is robust to the boundary polygon selection process, satisfying Property 1. Fig. 4 shows that the precision matrix is very sparse. The computationally demanding operation when using the Barrier SGF is a repeated Cholesky factorisation, which is a factorisation of a matrix with the same sparsity structure as for the stationary SGF, resulting in the same computational cost, $\mathcal{O}(n^{3/2})$ where n is the number of nodes in the finite element mesh (Lindgren et al., 2011), hence the Barrier SGF satisfies Property 2.

The only step that needs to be assessed by the user is the step of mesh construction, including whether the boundaries have a reasonable representation in the mesh, but this step is also needed when using the stationary SGF.
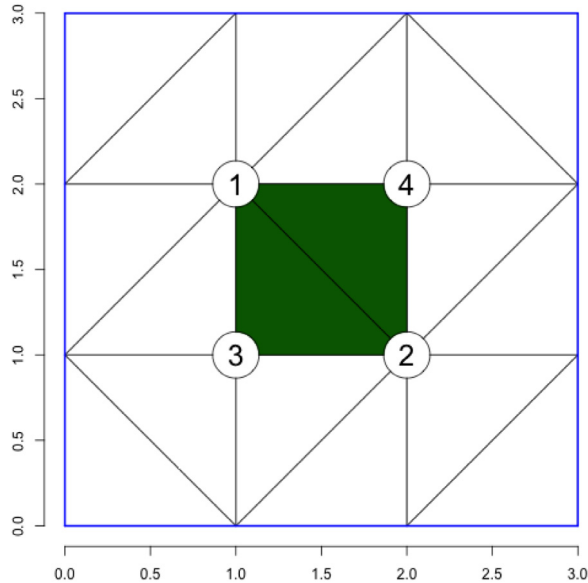
Fig. 5. Example simple mesh used for computing example D_q matrices in Section 3.
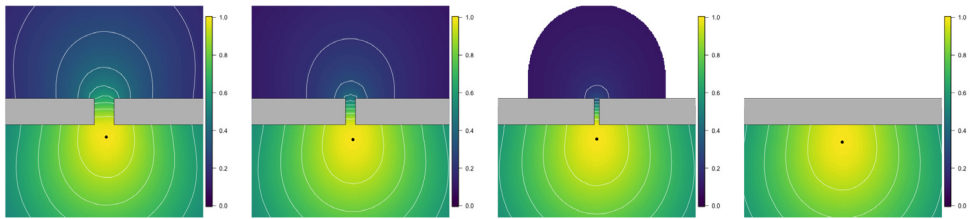

Fig. 6. Correlation plots of the same scenarios as in Fig. 3, showing that the Barrier SGF is also robust to the boundary polygon selection process.

For the marginal standard deviation of the field at a location s we have two options. One is to use the spatially varying standard deviation we get from solving the above equations, which results in higher prior standard deviation in inlets. The second option is to rescale the precision matrix so that all the marginal standard deviations are 1. This can be done by finding the marginal variances (finding the inverse diagonal of the precision matrix through sparse computations), and rescaling the precision matrix using these values. In this paper, we have chosen the first option mainly for its interpretation; we believe that this non-constant marginal spatial uncertainty is *a priori* reasonable. The SGF is a solution to an SPDE and represents the "average location" of a randomly moving individual in the physical space defined by the differential equation. E.g. in the archipelago example, narrow inlets are places that an individual is less likely to visit as opposed to the large open sea areas but if the individual gets into an inlet, it will remain in there for a longer period. This leads to higher standard deviations compared to a stationary SGF; e.g. either there is a lot of fish, or there are almost no fish, in the inlet.

4. The modified Horseshoe reconstruction problem

In this section we illustrate the difference between the stationarity assumption, the Neumann assumption, and the new model, through reconstructing a known test surface, and we study whether
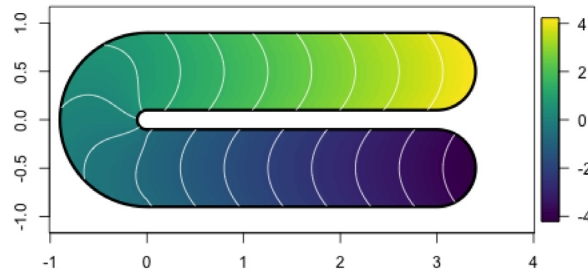
Fig. 7. The true function that is to be reconstructed in the modified horseshoe example. The white lines are height curves at regular intervals.

the gain in reconstruction quality when using the new model is substantial or minor. The original Horseshoe test surface was developed by Ramsay (2002), but happens to fulfil the Neumann boundary condition, and so, any approach satisfying the Neumann boundary condition has unfairly good performance. To fix this, Wood et al. (2008) modified the test function so that it did not have any of the typical boundary conditions (Dirichlet or Neumann), see Fig. 7 for this test function.

We compare reconstructions from three different models, all of them hierarchical Bayesian models with Gaussian observation noise, fitted with R-INLA (Rue et al., 2017). In this paper we use the term "model" for the entire prior model, including observation likelihood, and the term SGF for the spatial component in the model, indexed by two hyper-parameters r and σ. MB is a model using the Barrier SGF (described in Section 2), MS is a model using the stationary SGF (with a large convex mesh), and MN is the Neumann model (mesh only defined in water). The main reasons for including MS in the comparison is that this is the most well known model, and the properties we set out in the introduction refer to the "stationary alternative". The main reason for including MN in the comparison is that it is the only current solution satisfying Properties 1 through 4, indeed, the only reason we do not consider this model to be a solution to the coastline problem, which would make the Barrier model superfluous, is that it introduces a new unrealistic assumption, as detailed in this section. The complete prior model specifications, together with rationale, can be found in the supplementary material. We also note that MS and MN are the two most commonly used models for coastlines in R-INLA today. We have chosen not to compare with any of the other approaches in the literature as they do not fulfil the required properties.

Fig. 8 shows sample reconstructions of Fig. 7 for all three models, computed as the posterior mean of the SGF. MS smooths over the gap, hence, in the areas near the gap the stationary reconstruction is only good if there is an observation in a location near the boundary. In general, if you have many observation locations along the entire boundary, the stationary reconstruction will look reasonable. MB gives a reconstruction that seems the most similar to the true surface, including height curves that behave similarly to the true height curves. In contrast to the true surface, MN has very straight height curves that are orthogonal to the boundary. Judging by these plots, the assumptions of MB seem more realistic than those of MS or MN when reconstructing an unknown function.

In the following simulation scenarios, locations were sampled uniformly at random for each run, and Gaussian noise with standard deviation σ_ϵ was added to the true values. Then the three models were fitted to the data and the posterior mean of the SGF (plus intercept) used as the reconstruction. For model comparison the root mean square error (RMSE) was used to measure the quality of the reconstruction. To study the variability of the reconstruction quality we simulate 1000 runs for each scenario, and show the results in Fig. 9. From these results we conclude that MB is the best model for reconstructing the true surface, and that this is statistically significant. The scale of the RMSE shows that the differences are also of large practical significance; the error of the Barrier SGF is less than half that of the stationary SGF for $\sigma_\epsilon = 0.1$. The least difference in RMSE we find is when we have a medium number of locations, and a large noise ($\sigma = 1, n = 600$), between the Barrier and Neumann SGFs, which might be due to the boundary assumption having less impact in the presence of a large measurement noise.

(a) MS reconstruction

(b) MB reconstruction

(c) MN reconstruction
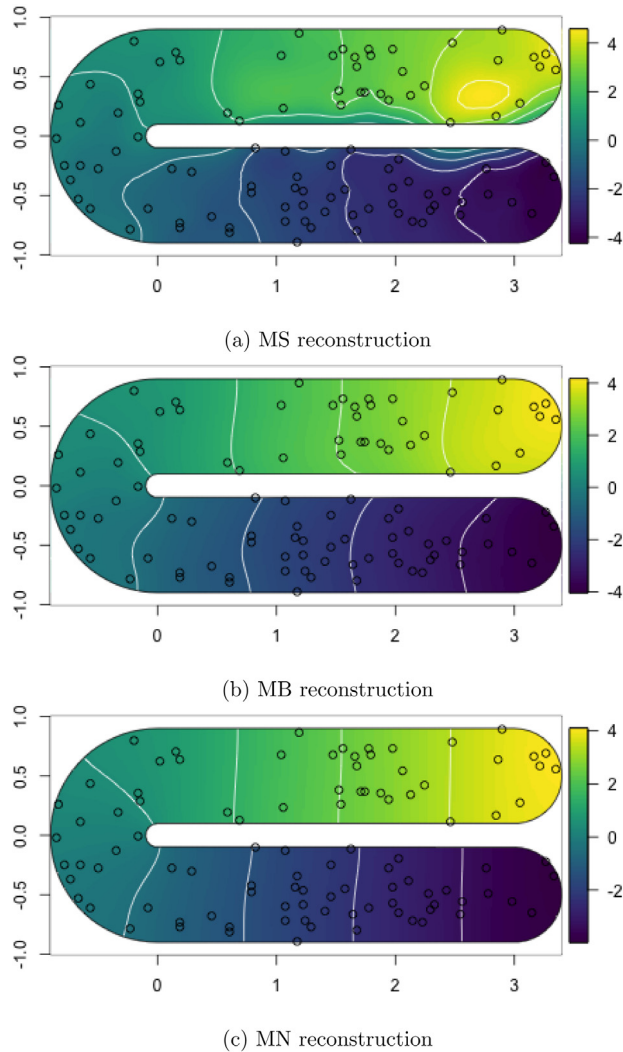
Fig. 8. The reconstruction estimates from the three different models. MS (The stationary SGF) smooths over the gap, the Barrier SGF gives a good reconstruction, and the Neumann SGF has height-curves that are orthogonal to the boundary.

The simulations for $\sigma = 0.1, n = 3000$ are particularly interesting. One might expect the boundary conditions to have less of an impact as n increases, but that is not the case, the gain made by the Barrier SGF does not seem to diminish as n increases. Interestingly, MN is better than MS for sparse data, but MN is significantly worse for richer data. With small sample size the informative Neumann boundary is beneficial, because this prior information contains more probability mass near the truth than the stationary prior. In MS the prior information on boundaries is very vague and hence data, through the likelihood, can update the SGF on the boundary a lot. However, as sample size increases the information from data starts to overrule the prior information in MS and the posterior mean approaches the true value. The Neumann boundary corresponds to prior information with zero uncertainty, hence this prior is not updated by any amount of data, and performs badly for rich
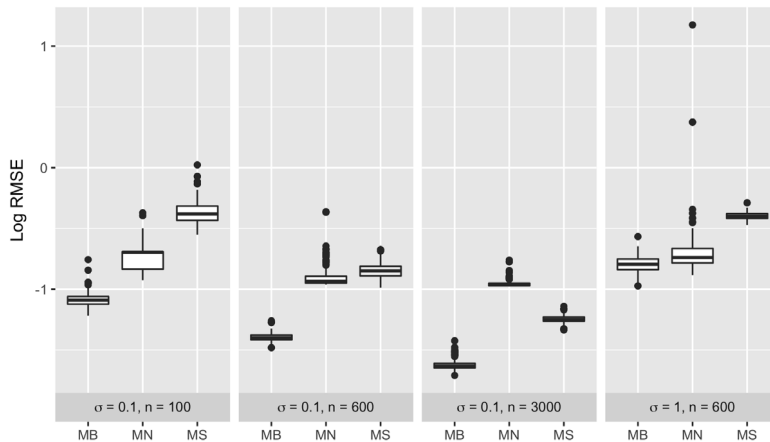
Fig. 9. A comparison of the RMSE when reconstructing the function in Fig. 7 from simulated random locations and random noise. Fig. 8 illustrates one reconstruction. MB uses the Barrier SGF, MN the Neumann SGF, MS the stationary SGF, and the logarithm is base 10.

datasets. In total, we conclude that the Neumann SGF does not satisfy Property 5 at all, as the results can be worse than when using a stationary SGF.

5. Modelling fish larvae in the Finnish Archipelago

In this application, which is the motivating example in the introduction, we model the spatial distribution fish larvae counts from the commercial fish species smelt, perch and pikeperch in the Archipelago Sea on the South-West coast of Finland. We have 198 observations of each species. Fig. 1 shows the study area and the observations for the smelt species, while a detailed description of the dataset is in Appendix B. The fish larvae are sensitive to habitat changes, therefore it is important to map the main density areas to protect the habitats when making management decisions. The motivation for analysing this dataset from the point of view of statistical model development is that the coastline is very complex, and the data very sparse, which makes it a challenging inference problem.

We use a hierarchical Bayesian model with over-dispersed Poisson likelihood, and priors that penalise complexity (Simpson et al., 2017; Fuglstad et al., 2015), see the supplementary material for the complete prior model specifications and rationale. The part of the prior model we focus on here is the priors for the stationary and Barrier SGFs, see Fig. 10 for spatial plots of the prior correlation. From the prior correlation we see that the stationary SGF smooths over land, while the Barrier SGF smooths around land, and is hindered by the presence of large and small islands. This is exactly the behaviour we desire from the Barrier SGF. Fig. 11 shows that the prior marginal standard deviation is slightly larger in narrow inlets, as discussed in Section 3. In total, we fit 6 different models to each dataset; with and without covariates, and with three different spatial components: Stationary SGF (model MS), Barrier SGF (model MB), and no spatial field (model MI).

Fig. 12 shows the posterior mean of the spatial component, in the models for smelt larvae without covariates. This illustrates the behaviour for datasets where there are no covariates, and datasets where the covariates are only able to model a small part of the data structure. In the figure we see the difference between the stationary SGF and the Barrier SGF, in how they smooth across land, e.g. around the peninsula in the north-east. The following Fig. 13 shows the difference in the spatial uncertainty estimation. In the south-east part of these plots we find inlets where we get higher uncertainty in the Barrier SGF compared to the stationary SGF. This is in accordance with our intuition, as we do not have much information about what happens there, because the coastline is separating the inlets from nearby measurement locations.
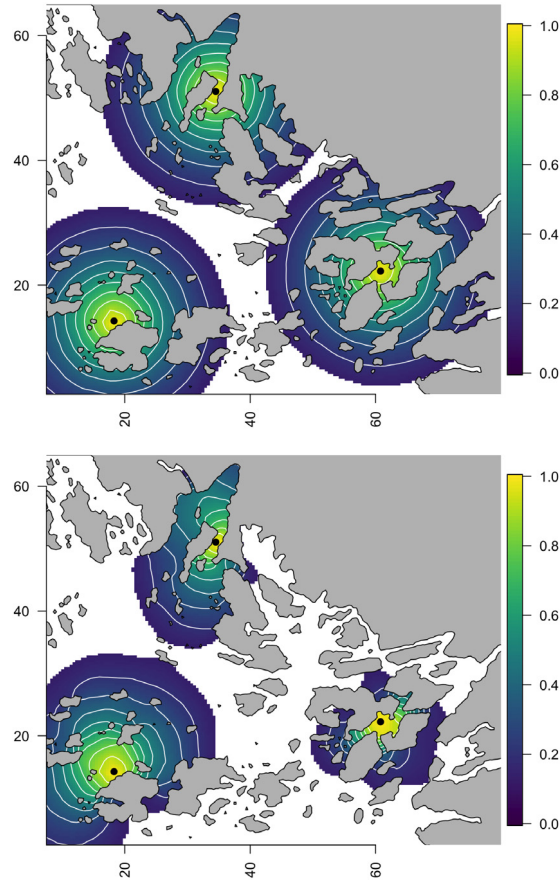
Fig. 10. This figure shows the prior behaviour of the new non-stationary Barrier SGF versus the stationary alternative. The map is of the Finnish Archipelago Sea, where water (white area) is considered as normal terrain, and land (grey area) is considered a physical barrier. The first plot shows three correlation surfaces for the stationary SGF with range $r = 18$ km. A correlation surface is the prior correlation between any point in the plane and a chosen central point (black dot). The correlation was cut off at 0.1. The second plot shows three correlation surfaces for the Barrier SGF, using the same range $r = 18$ km in the water area, and $r_b = 3.6$ km on land. Equidistant height curves are marked by white lines.

Fig. 14 summarises the point estimates and 95% credible intervals for the fixed effects in the models of smelt larvae. The posterior mean and intervals change from a model with no SGF to any of the spatial models, because the covariates are all spatially structured, hence confounded with the spatial model component. This confounding is desirable as it accounts for unmeasured covariates and spatial noise, making the fixed effects more reliable for extrapolation to other regions or other studies. We also observe changes in the posterior intervals between the model with stationary SGF (MS) and the model with Barrier SGF (MB). These changes may not be large enough to motivate the use of a very resource intensive non-stationary SGF, but considering the ease of use of the Barrier SGF, they are large enough that we recommend this non-stationary SGF for future applications. For completion, we show the results for the perch and the pikeperch larvae datasets in the supplementary material.

To investigate whether any of the datasets have a clear preference for one of the models, we compare all 6 models for each of the 3 species. The comparison criterion we use is Leave-One-Out Cross-Validation (LOOCV) with negative log predictive density (NLPD), and we bootstrap the mean score differences to understand the variability. A simpler scoring method would give us an estimate
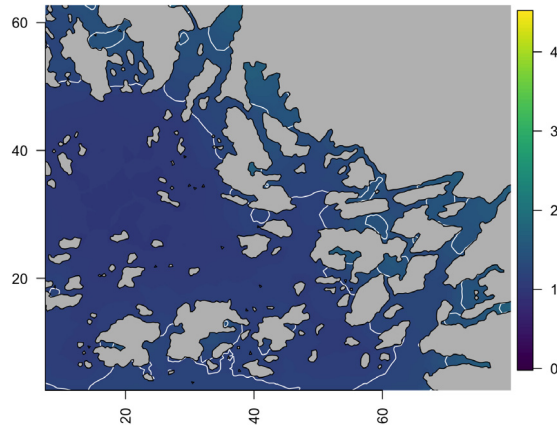
Fig. 11. Example prior marginal standard deviation of the Barrier SGF, using range 18 km in the water and range 3.6 km on land. This plot is on the same scale as we later use in Fig. 13.

of which model is best, but would be less reliable. We compute the score by running each model 198 times for each dataset, see the supplementary material. The results of this model comparison are almost all inconclusive, except for the result that the models with only intercept and iid effect are bad, all other models are approximately equally good, as the zero level is within the variability of the comparison criterion.

We now argue that property 3 is satisfied by the Barrier SGF. From the LOOCV, together with the inference performed in Section 4 and extensive informal experimentation, we conclude that models based on the Barrier SGF are numerically stable, as we have not encountered cases where a model with the Barrier SGF failed to converge but one with the stationary SGF succeeded. A simulation study in the archipelago can be found in the supplementary material.

6. Discussion

In statistics, one of the main aims is to construct realistic models that are motivated by common sense and scientific knowledge. In spatial modelling, classical models are unrealistic when they smooth over holes or physical barriers, and thus, to address these issues, statisticians have developed several more realistic models. However, realism alone may not be sufficient; if the improved models have other weaknesses, compared to the classical models, they may not always be useful. So far, there seems to be a trade-off, in that more realistic models are much more time consuming to fit and/or more complex to use, and/or introduce new unrealistic assumptions, compared to the classical models. The achievement in this paper is that we developed a new realistic approach, the Barrier model, that does not have this trade-off. As highlighted by the five properties we defined, the new model seems to have no practical weaknesses. Therefore, users can use it in all application scenarios, including those with sparse data and very complex boundaries.

The primary advantage of the Barrier SGF compared to previous approaches is the computational efficiency. Through the SPDE formulation, we achieve a computational cost equal to the stationary model, in theory, because we obtain the same sparsity structure for the precision matrix of the Barrier SGF as for the stationary SGF. The current implementation of the Barrier model is in R, and the stationary model is in C, leading to different computational times between the two models when using the code provided in the supplementary material. This efficiency allows us to perform thousands of simulation-inference runs in Section 4, a cross-validation study for the Archipelago application (see supplementary material), and a simulation study for the Archipelago (see supplementary material). Further, using these precision matrices in R-INLA is fast for datasets with a hundred thousand

(a) Stationary model (MS)


(b) Barrier model (MB)
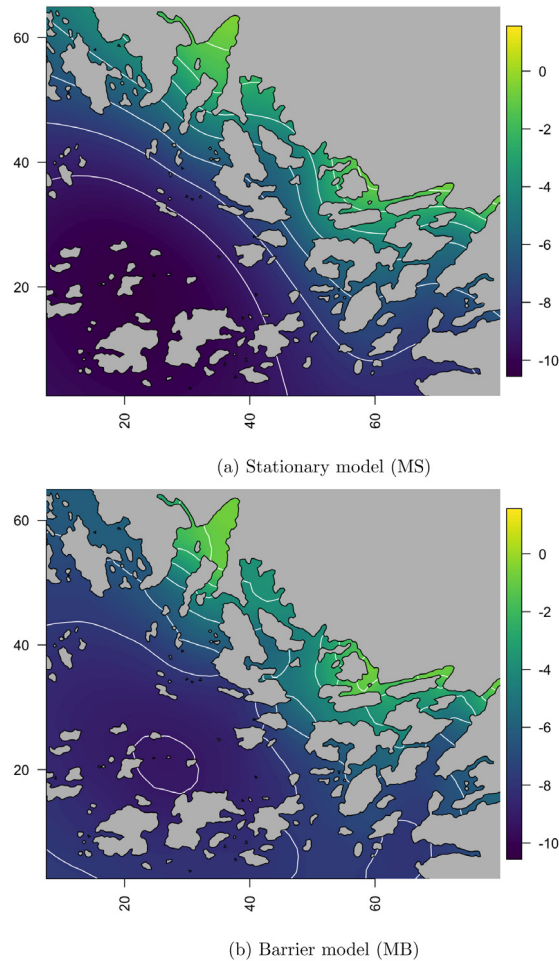
Fig. 12. Posterior mean estimate of the spatial field for the smelt larvae in the models without covariates. We see how MS smooths over the peninsula in the northern part of the figure, while MB does not.

observations, and allows us to construct space–time models defined as Kronecker products of the Barrier SGF and a temporal model.

In this paper we also discuss whether the inference results are different enough, between the stationary model and the Barrier model, to recommend using the model in practice. For reconstructing the horseshoe test function, we get large differences, similarly to the existing literature (e.g. Wood et al. (2008)). For this example it is clear that neither the stationary nor the Neumann model can be used, and an improved model is needed. However, we caution against comparing advanced approaches to the coastline problem by their performance on this single test function. Similarly to how the original test function preferred models with Neumann boundary assumption (Wood et al., 2008), the current Horseshoe prefers a specific type of models. The "winner" of a comparison based on any single example would mostly be determined by which approach has the most similar prior (or null-space, or "low penalty space") to the true boundary of the Horseshoe function. Comparing different approaches to the coastline problem must be done with greater care, and we would like to see defined a collection of different test functions, with different coastlines, satisfying very different boundary conditions, to get a more general comparison criterion.

(a) Stationary model (MS)

(b) Barrier model (MB)
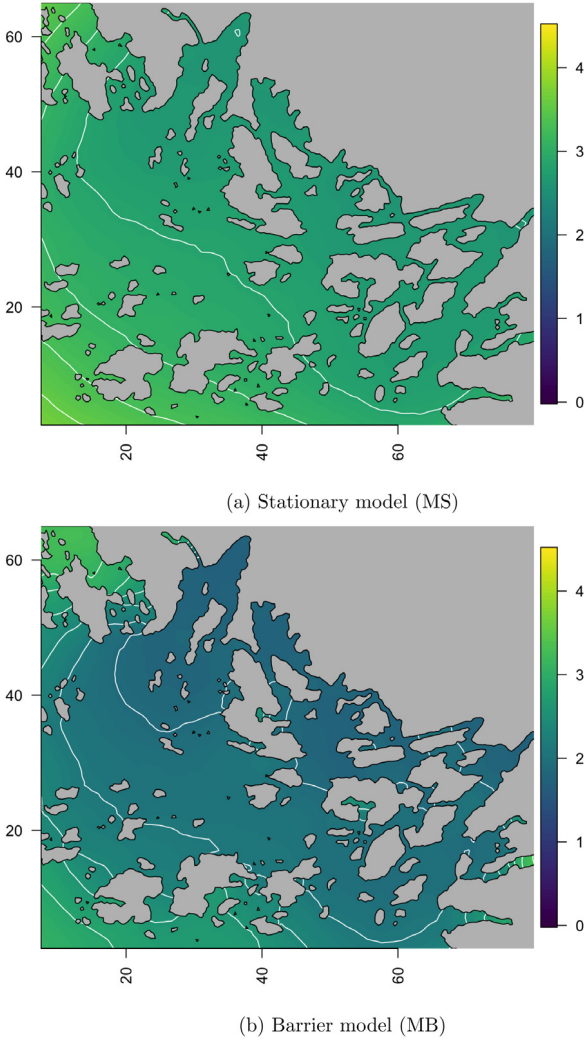
Fig. 13. Posterior spatial uncertainty (marginal standard deviation) for the smelt larvae in the models without covariates. We see that the uncertainty in MB is lower over all, but larger in inlets.

In the Archipelago application, the field is sparsely observed, and so, the posterior SGF changes substantially between the stationary SGF and the Barrier SGF. When visualising (smoothing) spatial data, scientists will not accept a visualisation that is intuitively inappropriate, as is the case with the result of the stationary SGF. In all applications where the spatial estimation maps are important we recommend using the Barrier model.

For applications where the main concern is estimating the coefficients of the fixed effect (or similar non-linear terms), and the SGF is a nuisance parameter, the difference between using a simple model and a model taking the coastline into account may be almost negligible. Based on the results in this paper, and experimentation with two other datasets, we cannot in general recommend the use of a complex and time consuming approach to the coastline problem. However, we can recommend using the Barrier model, as the time and effort required to fit this model is almost the same as for the stationary model.
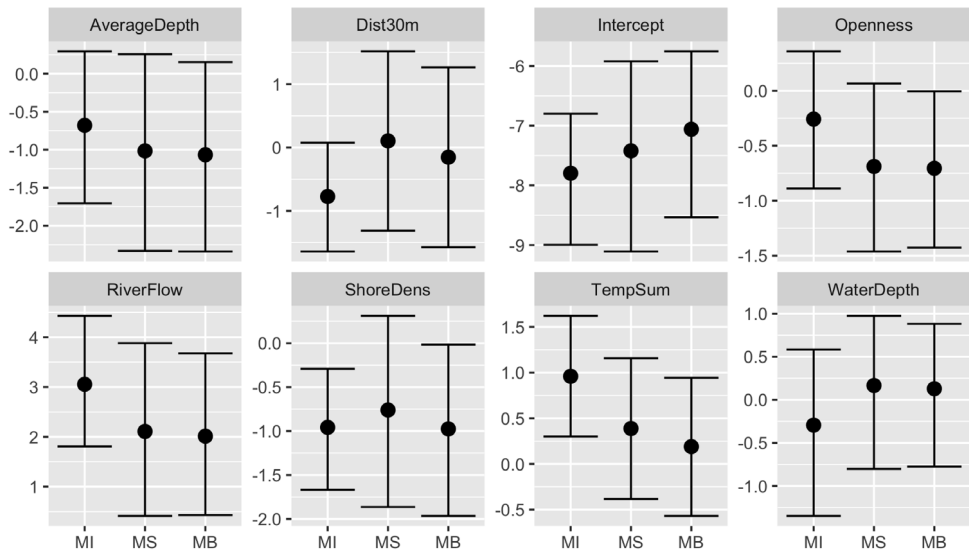
Fig. 14. A comparison of the posterior medians and 95% credible intervals for the fixed effects in the smelt analysis between three models. MI is the model without spatial field, MS the model with stationary SGF, and MB the model with Barrier SGF.

The weaker points of the results in this paper are the arbitrariness of the choice of range fraction r_b/r, and the inability to deal with physical barriers that are infinitely thin. Ad-hoc sensitivity analysis showed that the fraction we chose had almost no impact on parameter estimation. The simulation study in the Archipelago (see supplementary material) showed that the choice of range fraction did not impact predictive performance. Furthermore, any concerned user can study the impact of this choice through plotting prior correlation surfaces, *before* any data is fitted. As a side note, since the impact of changing this parameter (the range fraction, alternatively r_b) is so small, we strongly advise against attempting to estimate it. For dealing with physical barriers that are infinitely thin, we suggest making the barriers artificially thicker, so that the width is at least one mesh triangle across, and to use a very small range fraction.

There are several avenues for future research. First, the equations we solved in Section 3 can be used to infer k parameters in a non-stationary model, and we are looking into whether there are interesting applications of such an approach. Second, the SPDE approach can be used to model time-varying physical barriers in a space–time model, for example when regions are closed for fishing to preserve species. Third, the discussion of boundary conditions can be carried out into the field of SAR/CAR models in general, for example in disease mapping.

We end with a small remark; the Barrier SGF is in one view more flexible than the stationary SGF, as its correlation function (from empirical evidence) is always approximately the same or lower than that of the stationary SGF; the Barrier SGF may decouple some observations compared to the stationary SGF, but it does not increase other dependencies, when using the same range r in both models.

Acknowledgements

Appendix A. Proof of Theorem 1

The operator L is clearly linear, self-adjoint and positive definite. From the decay of the eigenvalues we get that L inverse is the limit of finite rank operators, hence L has a compact inverse. In total, L satisfies all the properties required for the results in Bolin et al. (2017). Define $\dot{H}^{-r}$ to be the dual space of $\dot{H}^r$ with respect to the inner product on the space H. From Lemma 2.1 in Bolin et al. (2017) there is a unique continuous extension of L to an isometric isomorphism from $\dot{H}^s$ to $\dot{H}^{s-2}$ for any s. Proposition 2.3 and Remark 2.4 detail how this proves existence and uniqueness of a solution of the SPDE

$$Lu = \mathcal{W}.$$

Further, for any $\epsilon > 0$ we get $u \in L_2(\Pi; \dot{H}^{1-\epsilon})$. In particular, $u \in L_2(\Pi; H)$.

We note that the results in Bolin et al. (2017) can also be used to study the behaviour of the FEM approximation.

Appendix B. The fish larvae dataset

In this appendix we provide a more detailed description of the fish larvae dataset.

The study area is located in the Archipelago Sea on the south-west coast of Finland in the northern Baltic Sea (Fig. 1). The Baltic Sea is one of the largest brackish water bodies in the world consisting of shallow, topographically complex and extensive archipelago rich in islands. Environmental gradients are typically strong, both north-southward and west-eastward along the coastline but also from inshore to offshore, e.g. spring-time temperature sum (see Table B.1) and turbidity vary strongly between inner bays and open water area due to the influence of river runoff. The archipelago and coastal areas host many essential biological processes such as fish reproduction. Hence, knowledge on the specific reproduction areas is of central importance in marine spatial planning and fisheries management (Vanhatalo et al., 2012; Kallasvuo et al., 2017).

As a case study we consider three species of fish, smelt (*Osmerus eperlanus*), perch (*Perca fluviatilis*) and pikeperch (*Sander lucioperca*). They are of freshwater origin and spawn in shallow coastal waters in low salinity estuaries and river mouths in the northern Baltic Sea (Shpilev et al., 2005; Bergström et al., 2014). They are fished commercially and are also highly sought after by recreational fishers. Our main interest is in the early-stage larvae, which are found relatively close to the spawning sites. We use a subset of data (198 sampling locations) introduced by Kallasvuo et al. (2017). The data were collected in 2007 and 2011 and comprise of the number of larvae per sampling location together with information on varying sampling effort (measured as the volume of water sampled). The environmental variables included six variables, which were available in GIS format in 50m resolution throughout the study area, and spatial coordinates (see Table B.1). Sampling year was also available, but not included, as there were only two unique values, and the exploratory data analysis did not indicate any differences between years. If the study had contained more years, it would have been natural to include a temporal model component in the model, as in Kallasvuo et al. (2017).

The covariates, except for RiverFlow, were standardised to have mean zero and variance 1 before the analysis. This was mainly done in order to facilitate interpretation of the estimates and the uncertainty of the fixed effects. This also implies that due to standardisation the priors act in the same way on all fixed effects. The response of smelt abundance along the covariate RiverFlow was step-like in the analysis of Kallasvuo et al. (2017), which comprised the whole coastline of Finland. In our sub-area, 193 sites out of all 198 sites took on a total of only two different values. It is unlikely that a meaningful linear relationship can be derived given these values, and hence, we recoded the covariate as a factor covariate in this study, where 0 represents the values below the average and 1 represents values greater than the average.

Appendix C. A small code example

In this appendix we provide a small code example to show the implementation needed by users of the Barrier SGF. The relevant part of the code for MS was

Table B.1

Covariates used in the models.

Name	Covariate description
AverageDepth	Average depth in a circle of 15 km; describes the water depth gradient in a large spatial scale.
Dist30m	Distance to 30 m (or more) depth zone; implicates location in the archipelago so that, e.g. sheltered inner bays are emphasised by this covariate.
RiverFlow	Square root of inverse distance to nearest river mouth weighted with annual average runoff; describes the influence of the river mouths and freshwater runoff.
lined15km	Shoreline length in a circle of 15 km; describes the effect of wind exposure and water exchange.
Openness	$\log_{10}$ of wave exposure; describes the degree of wave exposure
TempSum	Cumulative temperature sum from ice-break to July 15; describes how rapidly water area warms up in spring after ice break-up.

```
>> spde = inla.spde2.pcmatern(mesh,
    prior.range = c(6, .5), prior.sigma = c(3, 0.01))
>> formula = y  -1+m + f(s, model=spde) +
    f(iidx, model="iid", hyper=hyper.iid)
```

while for MB we replace that code with

```
>> barrier.model = inla.barrier.pcmatern(mesh, barrier.triangles,
    prior.range = c(6, .5), prior.sigma = c(3, 0.01))
>> formula = y  -1+m + f(s, model=barrier.model) +
    f(iidx, model="iid", hyper=hyper.iid)
```

where `barrier.triangles` is a list of indices of the mesh triangles covering land.

Appendix D. Tutorials and supplementary material

The Barrier SGF is implemented in the R package **INLA**, as `inla.barrier.pcmatern`, and the main step needed, compared to fitting a stationary model, is to specify which part of the study area is the physical barrier, e.g. by a polygon. See the code examples and dataset at https://haakonbakka.bit bucket.io/btopic107.html and https://haakonbakka.bitbucket.io/btopic110.html.

Supplementary material related to this article can be found online at https://doi.org/10.1016/j. spasta.2019.01.002. This material includes additional details on the models, additional analyses, and additional model comparisons.

References

Bakka, H., 2018. How to solve the stochastic partial differential equation that gives a Matérn random field using the finite element method. arXiv preprint arXiv:1803.03765.

Bergström, U., Sundblad, G., Sandström, A., Eklöv, P., 2014. Nursery habitat availability limits adult stock sizes of predatory coastal fish. ICES J. Mar. Sci. 71, 672–680.

Bhatt, S., Weiss, D.J., Cameron, E., Bisanzio, D., Mappin, B., Dalrymple, U., Battle, K.E., Moyes, C.L., Henry, A., Eckhoff, P.A., Wenger, E.A., Briët, O., Penny, M.A., Smith, T.A., Bennett, A., Yukich, J., Eisele, T.P., Griffin, J.T., Fergus, C.A., Lynch, M., Lindgren, F., Cohen, J.M., Murray, C.L.J., Smith, D.L., Hay, S.I., Cibulskis, R.E., Gething, P.W., 2015. The effect of malaria control on plasmodium falciparum in Africa between 2000 and 2015. Nature (526), 207–211.

Blangiardo, M., Cameletti, M., 2015. Spatial and Spatio-Temporal Bayesian Models with R-INLA. John Wiley & Sons.

Bolin, D., Kirchner, K., 2018. The rational SPDE approach for Gaussian random fields with general smoothness. arXiv preprint a rXiv:1711.04333.

Bolin, D., Kirchner, K., Kovács, M., 2017. Numerical solution of fractional elliptic stochastic pdes with spatial white noise. arXiv preprint arXiv:1705.06565.

Diggle, P.J., 2010. Historical introduction. In: Gelfand, A., Diggle, P., Fuentes, M., Guttorp, P. (Eds.), Handbook of Spatial Statistics. CRC/Chapman & Hall, Boca Raton, FL, pp. 3–16.

Fuglstad, G.-A., Simpson, D., Lindgren, F., Rue, H., 2015. Interpretable priors for hyperparameters for gaussian random fields. arXiv preprint arXiv:1503.00256.

Gander, M.J., Dubois, O., 2015. Optimized Schwarz methods for a diffusion problem with discontinuous coefficient. Numer. Algorithms 69 (1), 109–144.

Golding, N., Burstein, R., Longbottom, J., Browne, A.J., Fullman, N., Osgood-Zimmerman, A., Earl, L., Bhatt, S., Cameron, E., Casey, D.C., et al., 2017. Mapping under-5 and neonatal mortality in Africa, 2000–15: a baseline analysis for the sustainable development goals. The Lancet 390 (10108), 2171–2182.

Grisvard, P., 1985. Elliptic Problems in Nonsmooth Domains. In: monographs and studies in mathematics., vol. 24, Pitman.

Illian, J.B., Sørbye, S.H., Rue, H., 2012. A toolbox for fitting complex spatial point process models using integrated nested Laplace approximation (INLA). Ann. Appl. Stat. 1499–1530.

Kallasvuo, M., Vanhatalo, J., Veneranta, L., 2017. Modeling the spatial distribution of larval fish abundance provides essential information for management. Can. J. Fish. Aquat. Sci. 74, 636–649.

Krainski, E.T., Gómez-Rubio, V., Bakka, H., Lenzi, A., Castro-Camilo, D., Simpson, D., Lindgren, F., Rue, H., 2018. Advanced Spatial Modeling with Stochastic Partial Differential Equations Using R and INLA. Chapman and Hall/CRC.

Lindgren, F., Rue, H., Lindström, J., 2011. An explicit link between Gaussian fields and Gaussian Markov random fields: the stochastic partial differential equation approach. J. R. Stat. Soc. Ser. B Stat. Methodol. 73 (4), 423–498.

Miller, D.L., Wood, S.N., 2014. Finite area smoothing with generalized distance splines. Environ. Ecol. Stat. 21 (4), 715–731.

Noor, A.M., Kinyoki, D.K., Mundia, C.W., Kabaria, C.W., Mutua, J.W., Alegana, V.A., Fall, I.S., Snow, R.W., 2014. The changing risk of Plasmodium falciparum malaria infection in Africa: 2000-10: a spatial and temporal analysis of transmission intensity. The Lancet 383 (9930), 1739–1747.

Ramsay, T., 2002. Spline smoothing over difficult regions. J. R. Stat. Soc. Ser. B Stat. Methodol. 64 (2), 307–319.

Rue, H., Martino, S., Chopin, N., 2009. Approximate bayesian inference for latent gaussian models by using integrated nested laplace approximations. J. R. Stat. Soc. Ser. B Stat. Methodol. 71 (2), 319–392.

Rue, H., Riebler, A., Sørbye, S.H., Illian, J.B., Simpson, D.P., Lindgren, F.K., 2017. Bayesian computing with INLA: a review. Annu. Rev. Stat. Appl. 4, 395–421.

Sangalli, L.M., Ramsay, J.O., Ramsay, T.O., 2013. Spatial spline regression models. J. R. Stat. Soc. Ser. B Stat. Methodol. 75 (4), 681–703.

Scott-Hayward, L.A.S., MacKenzie, M.L., Donovan, C.R., Walker, C., Ashe, E., 2014. Complex region spatial smoother (CReSS). J. Comput. Graph. Statist. 23 (2), 340–360.

Shpilev, H., Ojaveer, E., Lankov, A., 2005. Smelt (Osmerus eperlanus L.) in the Baltic Sea. PProc. Est. Acad. Sci. Biol. Ecol. 54, 230–241.

Simpson, D., Rue, H., Riebler, A., Martins, T.G., Sørbye, S.H., 2017. Penalising model component complexity: A principled, practical approach to constructing priors. Statist. Sci. 32 (1), 1–28.

Vanhatalo, J., Veneranta, L., Hudd, R., 2012. Species distribution modelling with gaussian processes: a case study with the youngest stages of sea spawning whitefish (Coregonus lavaretus L. s.l.) larvae. Ecol. Model. 228, 49–58.

Wang, H., Ranalli, M.G., 2007. Low-rank smoothing splines on complicated domains. Biometrics 63 (1), 209–217.

Whittle, P., 1954. On stationary processes in the plane. Biometrika 41 (3/4), 434–449.

Wood, S.N., Bravington, M.V., Hedley, S.L., 2008. Soap film smoothing. J. R. Stat. Soc. Ser. B Stat. Methodol. 70 (5), 931–955.